Lawrence Berkeley National Laboratory
LBL Publications

Title
Limits on the Low-energy Electron Antineutrino Flux from the Brightest Gamma-Ray Burst of All Time

Permalink
https://escholarship.org/uc/item/4f60285c

Journal
The Astrophysical Journal, 981(2)

ISSN
0004-637X

Authors
Abe, S
Araki, T
Chauhan, S
et al.

Publication Date
2025-03-10

DOI
10.3847/1538-4357/ad9c36

Peer reviewed

eScholarship.org Powered by the California Digital Library
University of California

The Astrophysical Journal, 981:192 (6pp), 2025 March 10 https://doi.org/10.3847/1538-4357/ad9c36
© 2025. The Author(s). Published by the American Astronomical Society.
OPEN ACCESS

Limits on the Low-energy Electron Antineutrino Flux from the Brightest Gamma-Ray Burst of All Time

S. Abe[1,24], T. Araki[1], S. Chauhan[1], K. Chiba[1], T. Eda[1], M. Eizuka[1], Y. Funahashi[1], A. Furuto[1], A. Gando[1], Y. Gando[1,2], S. Goto[1], T. Hachiya[1], K. Hata[1], K. Ichimura[1], H. Ikeda[1], K. Inoue[1], K. Ishidoshiro[1], Y. Kamei[1,25], N. Kawada[1], Y. Kishimoto[1], M. Koga[1,3], A. Marthe[1], Y. Matsumoto[1], T. Mitsui[1,26], H. Miyake[1,4], D. Morita[1], R. Nakajima[1], K. Nakamura[1,27], R. Nakamura[1], R. Nakamura[1], J. Nakane[1], T. Ono[1], H. Ozaki[1], K. Saito[1], T. Sakai[1], I. Shimizu[1], J. Shirai[1], K. Shiraishi[1], A. Suzuki[1], K. Tachibana[1], K. Tamae[1], H. Watanabe[1], K. Watanabe[1], S. Kurosawa[5], Y. Urano[5], S. Yoshida[6], S. Umehara[7], K. Fushimi[5], K. Kotera[8], B. E. Berger[9], B. K. Fujikawa[3,9], J. G. Learned[10], J. Maricic[11], Z. Fu[12], S. Ghosh[8], J. Smolsky[8], L. A. Winslow[8], Y. Efremenko[3,13], H. J. Karwowski[14,15,16,17], D. M. Markoff[14,15,16,17], W. Tornow[3,14,15,16,17], S. Dell'Oro[18], T. O'Donnell[18], J. A. Detwiler[14,19], S. Enomoto[14,19], M. P. Decowski[20], K. M. Weerman[20], C. Grant[21], Ö. Penek[21], H. Song[21], A. Li[22], S. N. Axani[23], M. Garcia[23], and M. Sarfraz[23]

The KamLAND Collaboration

[1] Research Center for Neutrino Science, Tohoku University, 980-8578, Japan
[2] Department of Human Science, Obihiro University of Agriculture and Veterinary Medicine, Obihiro, Hokkaido 080-8555, Japan
[3] Kavli Institute for the Physics and Mathematics of the Universe (WPI), The University of Tokyo Institutes for Advanced Study, The University of Tokyo, Kashiwa, Chiba 277-8583, Japan
[4] Graduate Program on Physics for the Universe, Tohoku University, Sendai 980-8578, Japan
[5] Institute for Materials Research, Tohoku University, Sendai, Miyagi, 980-8577, Japan
[6] Graduate School of Science, Osaka University, Toyonaka, Osaka 560-0043, Japan
[7] Research Center for Nuclear Physics, Osaka University, Ibaraki, Osaka 567-0047, Japan
[8] Graduate School of Integrated Arts and Sciences, Tokushima University, Tokushima 770-8502, Japan
[9] Nuclear Science Division, Lawrence Berkeley National Laboratory, Berkeley, CA 94720, USA
[10] Department of Physics and Astronomy, University of Hawaii at Manoa, Honolulu, HI 96822, USA
[11] Department of Physics, Tokushima University, Tokushima 770-8506, Japan
[12] Massachusetts Institute of Technology, Cambridge, MA 02139, USA
[13] Department of Physics and Astronomy, University of Tennessee, Knoxville, TN 37996, USA
[14] North Carolina Central University, Durham, NC 27707, USA
[15] The University of North Carolina at Chapel Hill, Chapel Hill, NC 27599, USA
[16] Triangle Universities Nuclear Laboratory, Durham, NC 27708, USA
[17] Physics Departments at Duke University, Durham, NC 27708, USA
[18] Center for Neutrino Physics, Virginia Polytechnic Institute and State University, Blacksburg, VA 24061, USA
[19] Center for Experimental Nuclear Physics and Astrophysics, University of Washington, Seattle, WA 98195, USA
[20] Nikhef and the University of Amsterdam, Science Park, Amsterdam, The Netherlands
[21] Boston University, Boston, MA 02215, USA
[22] Halıcıoğlu Data Science Institute, Department of Physics, University of California San Diego, La Jolla, CA 92093, USA
[23] Department of Physics and Astronomy, University of Delaware, Newark, DE 19716, USA; milesg@udel.edu
Received 2024 October 3; revised 2024 December 2; accepted 2024 December 7; published 2025 March 7

Abstract

The electron antineutrino flux limits are presented for the brightest gamma-ray burst (GRB) of all time, GRB221009A, over a range of 1.8–200 MeV using the Kamioka Liquid Scintillator Antineutrino Detector. Using multiple time windows ranging from minutes to days surrounding the event to search for electron antineutrinos coincident with the GRB, we set an upper limit on the flux under the assumption of several power-law neutrino source spectra, with power-law indices ranging from 1.5 to 3 in steps of 0.5. No excess was observed in any time windows ranging from seconds to days around the event trigger time T_0. For a power-law index of 2 and a time window of $T_0 \pm 500$ s, a flux upper limit of $2.34 \times 10^9\,\mathrm{cm}^{-2}$ was calculated. The limits are compared to the results presented by IceCube.

Unified Astronomy Thesaurus concepts: Gamma-ray bursts (629); Neutrino astronomy (1100)

1. Introduction

On 2022 October 9, gamma-ray detectors observed an extremely bright gamma-ray burst (GRB) adjacent to the Galactic plane on the sky. This event, GRB221009A, was first observed by the Fermi Gamma-ray Burst Monitor (Fermi-GBM) at 13:16:59.99 UT (S. Lesage et al. 2022) and was soon followed by observations from the SWIFT Burst Alert Telescope (BAT) and X-Ray Telescope (XRT; S. Dichiara et al. 2022), as well as the Fermi Large Area Telescope (Fermi-LAT; E. Bissaldi et al. 2022), with further observations from

[24] Present address: Kamioka Observatory, Institute for Cosmic-RayResearch, The University of Tokyo, Hida, Gifu 506-1205, Japan.
[25] Present address: Center for Advanced Photonics, RIKEN, Wako, Saitama, 351-0198, Japan.
[26] Present address: Faculty of Health Sciences, Butsuryo College of Osaka, Sakai, Osaka 593-8328, Japan.
[27] Present address: Faculty of Environmental and Urban Engineering, Kansai University, 3-3-35 Yamate, Suita, Osaka, 564-8680, Japan.

Original content from this work may be used under the terms of the Creative Commons Attribution 4.0 licence. Any further distribution of this work must maintain attribution to the author(s) and the title of the work, journal citation and DOI.

Konus-Wind and INTEGRAL (D. Svinkin et al. 2022). The GRB was classified as a long GRB (duration more than 2 s), and its position was triangulated by the InterPlanetary Network (D. Svinkin et al. 2022). The initial light curve from Fermi-GBM showed a short pulse at the time of the initial trigger (T_0), followed by an extremely bright and long pulse starting 221 s after T_0. T_{90}, the time for 90% of the energy in gamma rays to be observed, was measured to be ~327 s. This was the brightest GRB ever recorded by Fermi-GBM (S. Lesage et al. 2022), saturating the detector for large parts of the second pulse. The position of the GRB, using data from SWIFT, was determined to be R.A. = 19^h 13^m 03^s, decl. = $+19^d$ 48' 09". The redshift of the GRB was determined 11.55 hr after T_0 by X-SHOOTER at the Very Large Telescope to be $z = 0.151$ (A. de Ugarte Postigo et al. 2022).

Follow-up analyses quickly confirmed the extreme energetics of GRB221009A. It was determined to have the highest fluence, peak flux, and equivalent isotropic energy ever recorded for a GRB (E. Burns et al. 2023). LHAASO announced the observation of the highest-energy photon from a GRB ever observed in coincidence with this event at more than 18 TeV, as well as 5000 very high energy (VHE: $E > 100$ GeV) photons from the event (Y. Huang et al. 2022), when only hundreds of VHE photons had ever been seen from GRBs previously. The full LHAASO analysis placed constraints on properties of the GRB, such as the jet opening angle and bulk Lorentz factor, that help explain GRB221009A's unique energetics (LHAASO Collaboration et al. 2023). Additionally, IceCube performed an analysis looking for neutrinos with energies between 0.5 and 10^6 GeV, but was not able to claim any significant observations (R. Abbasi et al. 2023, 2024).

Prior to this analysis, the Kamioka Liquid Scintillator Antineutrino Detector (KamLAND) has performed astrophysical searches looking for neutrinos coincident with GRBs (S. Abe et al. 2022b), as well as gravitational waves (S. Abe et al. 2021), solar flares (S. Abe et al. 2022c), and supernovae (S. Abe et al. 2022d), placing the most stringent limits on the neutrino flux from GRBs at low energies ($E < 100$ MeV). In this paper, we perform a time-coincident neutrino search using KamLAND to calculate the electron antineutrino flux from GRB221009A at the lowest energies from 1.8 to 200 MeV using various time windows, covering seconds to days surrounding the event, and assuming a power-law energy spectrum for the neutrinos produced at the source, with power-law indices ranging from 1.5 to 3 in steps of 0.5.

2. Neutrino Emission from GRBs

GRBs are some of the most energetic electromagnetic phenomena in the Universe. Long GRBs result from core-collapse supernovae (D. Xu et al. 2013) and are expected to release a large amount of energy ($\mathcal{O}(10^{53}$ erg)) (J.-L. Atteia et al. 2017, 2018) with neutrinos emitted over a large range of energies from MeV to EeV. The prompt gamma-ray emission of GRBs is thought to come from the dissipation of kinetic energy in relativistic fireballs by internal shocks (M. J. Rees & P. Meszaros 1994), as well as magnetic reconnection in the resulting relativistic outflow (P. Mészáros & M. J. Rees 1997). While accelerated electrons produce the gamma rays associated with the GRBs via synchrotron emission, accelerated protons and neutrons in the outflow can produce high energy (TeV–PeV) neutrinos by interacting with photons (E. Waxman & J. Bahcall 1997; J. K. Becker et al. 2006; K. Murase & S. Nagataki 2006; S. Hümmer et al. 2012; M. Bustamante et al. 2015; D. Biehl et al. 2018; T. Pitik et al. 2022; S. Ai & H. Gao 2023; R.-Y. Liu et al. 2023; A. Rudolph et al. 2023). Additionally, GeV neutrinos may be generated by proton and neutron interactions prior to gamma-ray emission (J. N. Bahcall & P. Mszros 2000; I. Bartos et al. 2013; K. Murase et al. 2013, 2022), and neutrinos with energies up to EeV may be produced by reverse shocks in the afterglow phase of the GRB (E. Waxman & J. N. Bahcall 2000; K. Murase 2007; J. K. Thomas et al. 2017; K. Murase et al. 2022; B. T. Zhang et al. 2023). At low (MeV) energies, neutrinos may be produced by quasi-thermal processes in the core collapse (M. D. Kistler et al. 2013), in neutrino-dominated accretion outflows (T. Liu et al. 2017; Y.-Q. Qi et al. 2022), and within the fireball (F. Halzen & G. Jaczko 1996). However, it is unclear as to the level each of these mechanisms plays in neutrino production, so time windows are often chosen to be long enough to account for the large uncertainties in the production mechanisms.

3. KamLAND Detector

KamLAND is a 1 kton liquid scintillator detector located 1 km underneath Mt. Ikenoyama in Gifu, Japan. The detector consists of an outer detector and an inner detector, shown in Figure 1 (left). The outer detector holds 3.2 ktons of water and functions as a water Cherenkov cosmic-ray veto for the inner detector. The inner detector itself is an 18 m diameter stainless steel tank lined with 554 20 inch and 1325 17 inch photomultiplier tubes (PMTs) with a smaller, 13 m diameter nylon and EVOH outer balloon of 1 kton of ultrapure liquid scintillator (80% dodecane, 20% pseudocumene) held inside the tank with ropes and buffer oil, which also acts as additional gamma-ray shielding. The innermost 12 m of the outer balloon is used as the fiducial volume for antineutrino detection. This setup gives reconstructed positional and energy uncertainties of $\sim 12\,\mathrm{cm}/\sqrt{E\,(\mathrm{MeV})}$ and $\sim 6.4\%/\sqrt{E\,(\mathrm{MeV})}$, respectively (A. Gando et al. 2013). KamLAND was originally built to detect neutrinos from Japan's nuclear reactors, as well as geoneutrinos (T. Araki et al. 2005; S. Abe et al. 2008; A. Gando et al. 2013), and started data collection in 2002 toward this end. Starting in 2011 October, a 3.08 m diameter inner balloon was installed inside the outer balloon, and filled with 326 kg of xenon-loaded liquid scintillator for the KamLAND-Zen 400 neutrinoless double beta decay experiment (A. Gando et al. 2016). From 2018 April to 2024 January, a 3.8 m diameter balloon was filled with 745 kg of xenon and inserted in place of the 3.08 m balloon for the KamLAND-Zen 800 experiment (Y. Gando et al. 2020, 2021; S. Abe et al. 2023).

4. Data Selection and Background Estimation

4.1. Electron Antineutrino Selection

KamLAND uses the inverse beta decay (IBD) process to detect electron antineutrino interactions: $\bar{\nu}_e + p \rightarrow e^+ + n$. When this process occurs in the outer balloon of the detector, it produces a delayed coincidence (DC) signal that KamLAND can detect. The positron generated in the interaction will emit photons via scintillation before almost immediately annihilating with an electron, giving a prompt signal of two 511 keV photons (E_p). The neutron produced in the interaction will be

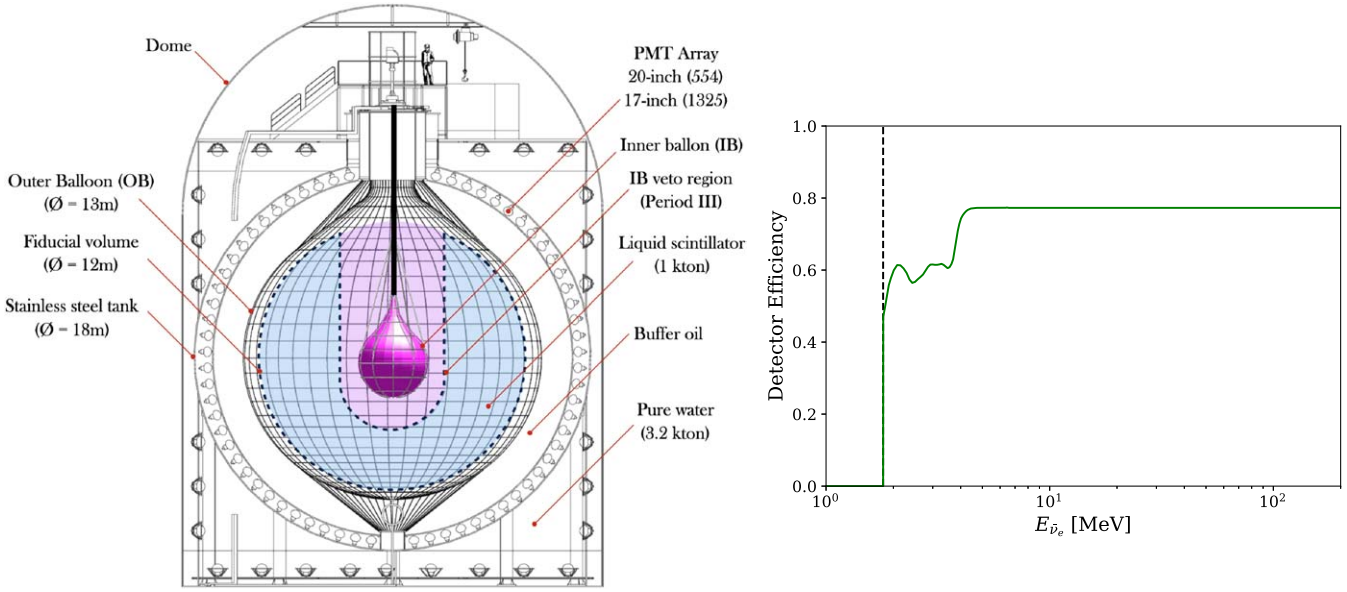

Figure 1. Left: a schematic diagram of the KamLAND detector during the KamLAND-Zen 800 experiment. The fiducial volume for $\bar{\nu}_e$ detection is highlighted in blue, while the inner balloon cut is shown in purple. The inner detector is azimuthally symmetric. Right: the IBD $\bar{\nu}_e$ detection efficiencies during the KamLAND-Zen 800 experiment. The structure below ~4 MeV arises from the likelihood selection. A vertical dotted line is shown at the 1.8 MeV low-energy IBD threshold.

Table 1
The Different Time Windows Used in the Analysis

Time Window	$\bar{\nu}_{e\text{obs}}$	N_{90}	Expected $\bar{\nu}_e$	F_{90} ($\gamma = 2$) (cm^{-2})	$E^2F_{90}(E)$ ($\gamma = 2$) (GeV cm^{-2})
T_0[+0, +327] s	0	2.44	0.001 ± 0.027	3.24×10^9	3.12×10^6
$T_0 \pm 500$ s	0	2.43	0.002 ± 0.047	3.23×10^9	3.11×10^6
T_0[−200, +2000] s	0	2.43	0.005 ± 0.070	3.23×10^9	3.11×10^6
T_0[−1, +2] hr	0	2.41	0.024 ± 0.155	3.21×10^9	3.10×10^6
$T_0 \pm 1$ day	0	2.05	0.381 ± 0.619	2.72×10^9	2.80×10^6
T_0[−1, +14] day	0	1.00	2.861 ± 1.690	1.33×10^9	1.34×10^6

Note. For each time window, the number of observed neutrinos, the signal upper limit, the number of $\bar{\nu}_e$ we expect to see from the background rate, the value of F_{90} for a power-law index of 2, and the calculated flux upper limit shown in Figure 3 for a power-law index of 2 are shown.

captured on a proton (carbon) with a mean capture time of 207.5 ± 2.8 μs, resulting in a delayed signal of a 2.22 (4.95) MeV photon (S. Abe et al. 2010). This DC pair is separated both in space ($\Delta R < 200$ cm) and time (0.5 μs $< \Delta T <$ 1000 μs). At low energies, the antineutrino energy can be approximated as the sum of the prompt energy (positron kinetic energy + annihilation energy = $2m_e$) + 0.782 MeV, ignoring the relatively small kinetic energy of the neutron (K. Asakura et al. 2015). To search for neutrinos at 200 MeV, we use the energy cut 0.9 MeV $< E_p <$ 200 MeV to conservatively cover uncertainties in the kinetic energy of the positron, the kinetic energy of the neutron, and energy scale uncertainties even if $\langle E_p \rangle = 172$ MeV. The DC temporal and spatial separation, as well as the known energies of the resulting photons, greatly reduces background signal contamination and results in a high detection efficiency at low energies.

To further isolate signal events, cuts are placed on the energy of the photon resulting from the neutron capture (E_d) such that 1.8 (4.4) MeV $< E_d <$ 2.6 (5.6) MeV for capture on protons (carbon). A further cut requires the DC pair to be found within a 6 m radius spherical volume in the center of the outer balloon. During the KamLAND-Zen experiment, an additional cut is used to avoid backgrounds from the inner balloon, removing a 2.5 m radial region around the vertical axis of the detector, extending from its top to its center, as well as a 2.5 m radius sphere around the center of the inner balloon. Finally, a likelihood-based selection is used to distinguish DC pairs from background events (A. Gando et al. 2013). GRB221009A took place during the KamLAND-Zen 800 experiment, so the inner balloon cut (the purple region in Figure 1) is included. The selection efficiency is shown in Figure 1 (right) and converges to 77.4% during this time, taking into account the loss in fiducial volume due to the inner balloon cut.

5. Time-coincident Event Search

We perform a time-coincident IBD search looking for antineutrino events in the detector that arrive in various time windows surrounding the GRB trigger time T_0. These windows cover timing differences in theoretical production mechanisms for neutrinos compared to photons, as well as the neutrino time-of-flight delay, with different time windows allowing the analysis to cover a wider range of possible production mechanisms. We choose time windows corresponding with the IceCube analysis, which cover potential precursor emission as well as gamma-ray emission observed by Fermi (E. Bissaldi et al. 2022; S. Lesage et al. 2022) and LHAASO (Y. Huang et al. 2022). These time windows are shown in Table 1. We

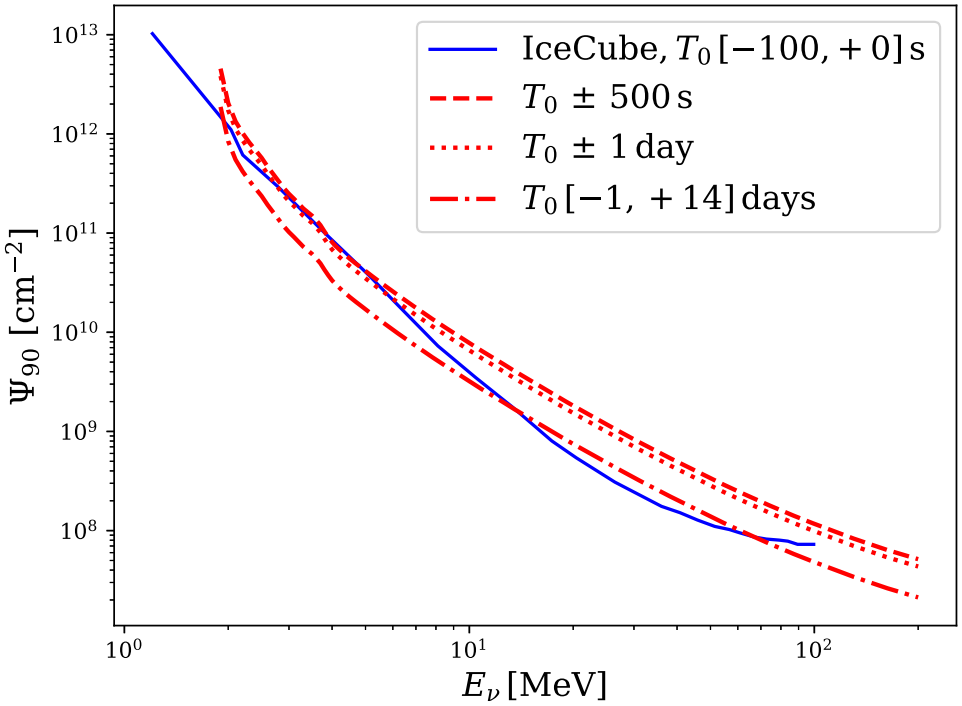

Figure 2. The KamLAND 90% confidence level model-independent Green's function as a function of energy between 1.8 and 200 MeV (red lines, different line styles correspond to different time windows) and IceCube ASTERIA 90% confidence level upper limit (blue). The other time windows in Table 1 are consistent with $T_0 \pm 500$ to within the linewidth. The KamLAND result is consistent with other nondetection KamLAND analyses, as in S. Abe et al. (2022a).

omit longer time windows since they are not as well motivated by the production mechanisms and do not significantly change the results. For each time window, we determine the number of IBD events observed by KamLAND, and then create the Feldman–Cousins confidence belt at the 90% confidence level (G. J. Feldman & R. D. Cousins 1998) from the number of observed IBD events in the time window, as well as the background rate in the detector. The primary backgrounds in the KamLAND IBD selection are neutrinos from the atmosphere, nuclear reactors, and radioactive decay in the Earth. To calculate the background rate, we look for IBD events over the whole of the KamLAND-Zen 800 period and divide that number by the detector livetime in that period. The expected number of observed IBD events can then be calculated for each time window. Model-independent antineutrino fluence limits are then computed with a Green's function using N_{90}, the upper bound of the Feldman–Cousins confidence belt, for each time window:

$$\Psi_{90}(E_{\bar{\nu}_e}) = \frac{N_{90}}{N_T \sigma(E_{\bar{\nu}_e}) \epsilon_{\text{live}}(E_{\bar{\nu}_e})}, \quad (1)$$

where N_T is the number of targets for IBD in the KamLAND detector, $\epsilon_{\text{live}}(E_{\bar{\nu}_e})$ is the detector efficiency, and $\sigma(E_{\bar{\nu}_e})$ is the IBD cross section (A. Strumia & F. Vissani 2003). Finally, the time-integrated antineutrino flux F_{90} is calculated for an assumed source emission model from 1.8 to 200 MeV:

$$F_{90} = \frac{N_{90}}{N_T \int \sigma(E_{\bar{\nu}_e}) \lambda(E_{\bar{\nu}_e}) \epsilon_{\text{live}}(E_{\bar{\nu}_e}) dE_{\bar{\nu}_e}}, \quad (2)$$

where $\lambda(E_{\bar{\nu}_e})$ is the normalized neutrino energy spectrum produced at the source. We choose power laws for this spectrum with indices from 1.5 to 3 in steps of 0.5 to be consistent with the IceCube analysis. These power-law indices are motivated by comparisons with gamma-ray and cosmic-ray production mechanisms, which produce power-law spectra with similar indices (P. Lipari & S. Vernetto 2020).

6. Results

The conservative neutrino time-of-flight delay from GRB221009A, assuming the heaviest neutrino mass of 59 meV, and base-ΛCDM cosmological parameters from N. Aghanim et al. (2020), was calculated to be ~30 s. We selected six time windows, shown in Table 1, that clearly account for the time-of-flight delay and allow for a wide range of neutrino production mechanisms. We did not observe any neutrinos within any of the chosen time windows. With zero observed neutrinos and a background rate we measured to be 2.23 μHz, the signal upper limits for each time window were calculated, and are shown in Table 1.

The model-independent Green's function is shown in Figure 2, where the band represents the space between the lowest and highest flux upper limits across the different time windows. This is compared to the IceCube low-energy model-independent flux upper limit (K. Kruiswijk et al. 2023), which was calculated using the IceCube ASTERIA low-energy simulation package (S. Griswold et al. 2020). This was calculated at similar energies to the neutrinos KamLAND can detect, giving a direct comparison of the two detectors' observation of the event.

Finally, we calculated the electron antineutrino flux F_{90} for each time window, assuming a power-law index of 2. These are shown in Table 1. We also calculate F_{90} for several power-law indices, ranging from 1.5 to 3 in steps of 0.5, using a time window of $T_0 \pm 500$ s. These results are compared with IceCube upper limits, as well as gamma-ray observations from Fermi, in Figure 3. These results are consistent with IceCube's

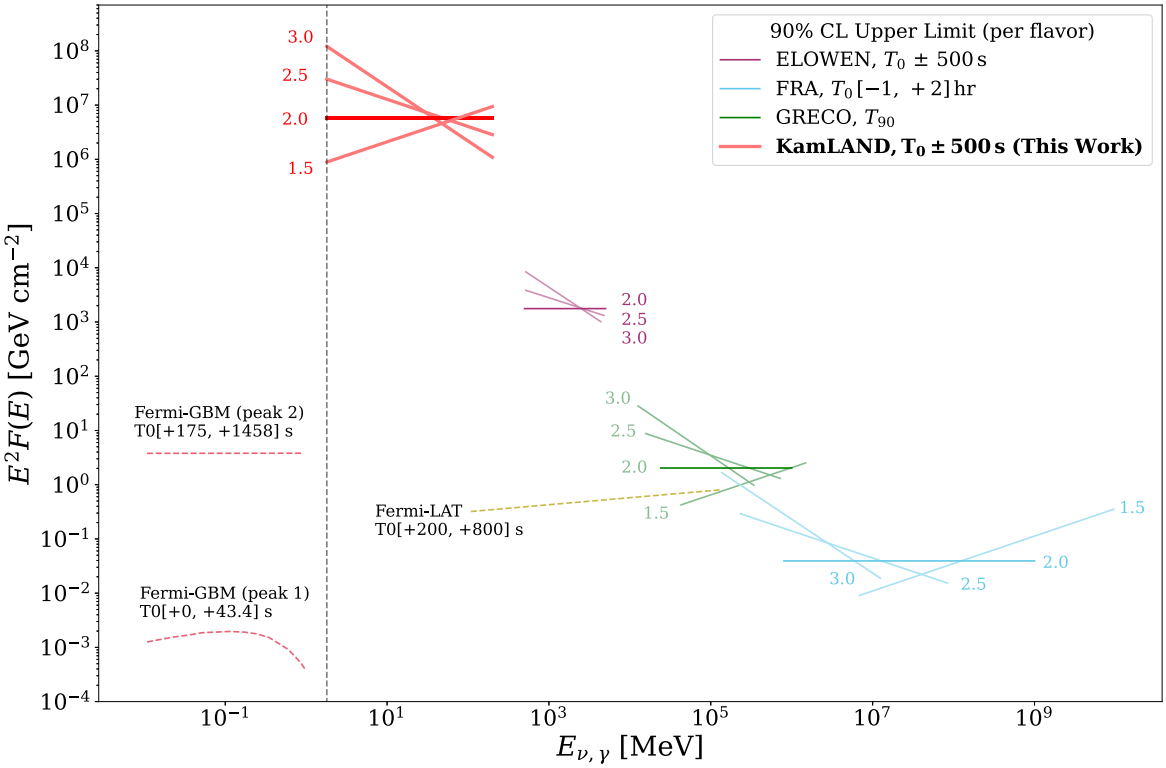

Figure 3. The 90% confidence level per-flavor neutrino flux from this work, shown in red, and IceCube analyses, shown in purple, green, and cyan (R. Abbasi et al. 2023, 2024). The horizontal dashed lines are gamma-ray observations (not upper limits) from Fermi. The vertical dashed line shows the IBD lower limit at 1.8 MeV. The curve labels identify the source emission power-law spectra, corresponding to the power-law index. The time windows for each curve are labeled. We chose $T_0 \pm 500$ s to match IceCube's ELOWEN analysis, as this was the lowest-energy IceCube result for a power-law source emission spectrum.

nonobservation of neutrinos from the GRB (R. Abbasi et al. 2023, 2024).

7. Discussion

GRB221009A has favorable properties, such as a small jet opening angle pointing at Earth (LHAASO Collaboration et al. 2023), so the lack of neutrino detection indicates that future events would need to be closer to Earth to stand a chance of being observed. Models for low-energy neutrino emission from GRBs exist for both isotropic and beamed emission, but the increase in flux from the beaming, without having been able to detect those neutrinos, means that it is unlikely to be possible to detect isotropic neutrino emission unless the event was extremely close to Earth.

Although we did not observe any neutrinos from GRB221009A, this analysis provides a pipeline for detecting neutrinos from future GRB events, as well as providing a useful benchmark for comparison, due to the unique energetics of GRB221009A.

8. Conclusion

We present a search for electron antineutrinos using the KamLAND detector between 1.8 and 200 MeV coincident with GRB221009A, the brightest GRB ever observed. We search for events within multiple time windows surrounding the GRB trigger time, corresponding to multiple possible $\bar{\nu}_e$ production mechanisms, as well as accounting for the neutrino time-of-flight delay. No coincident antineutrinos are found, but we are able to set upper limits on the $\bar{\nu}_e$ flux from the GRB using multiple source emission spectra. These limits, as well as model-independent limits, are compared to limits placed by IceCube and are found to be comparable.

Acknowledgments

The KamLAND-Zen experiment is supported by JSPS KAKENHI grant Nos. 21000001, 26104002, 24H02237, and 19H05803; the U.S. National Science Foundation award Nos. 2110720 and 2012964; the Heising-Simons Foundation; the Dutch Research Council (NWO); and under the U.S. Department of Energy (DOE) grant No. DE-AC02-05CH11231, as well as other DOE and NSF grants to individual institutions. The Kamioka Mining and Smelting Company has provided service for activities in the mine. We acknowledge the support of NII for SINET4.

References

Abbasi, R., Ackermann, M., Adams, J., et al. 2023, ApJL, 946, L26
Abbasi, R., Ackermann, M., Adams, J., et al. 2024, ApJL, 970, L43
Abe, S., Asami, S., Eizuka, M., et al. 2022a, APh, 143, 102758
Abe, S., Asami, S., Eizuka, M., et al. 2023, PhRvL, 130, 051801
Abe, S., Asami, S., Gando, A., et al. 2021, ApJ, 909, 116
Abe, S., Asami, S., Gando, A., et al. 2022b, ApJ, 927, 69
Abe, S., Asami, S., Gando, A., et al. 2022c, ApJ, 924, 103
Abe, S., Asami, S., Gando, A., et al. 2022d, ApJ, 925, 14
Abe, S., Ebihara, T., Enomoto, S., et al. 2008, PhRvL, 100, 221803
Abe, S., Enomoto, S., Furuno, K., et al. 2010, PhRvC, 81, 025807
Aghanim, N., Akrami, Y., Ashdown, M., et al. 2020, A&A, 641, A6
Ai, S., & Gao, H. 2023, ApJ, 944, 115
Araki, T., Enomoto, S., Furuno, K., et al. 2005, Natur, 436, 499
Asakura, K., Gando, A., Gando, Y., et al. 2015, ApJ, 806, 87
Atteia, J.-L., Heussaff, V., Dezalay, J.-P., et al. 2017, ApJ, 837, 119
Atteia, J.-L., Heussaff, V., Dezalay, J.-P., et al. 2018, ApJ, 852, 144
Bahcall, J. N., & Mszros, P. 2000, PhRvL, 85, 1362

Bartos, I., Beloborodov, A. M., Hurley, K., & Márka, S. 2013, PhRvL, 110, 241101
Becker, J. K., Stamatikos, M., Halzen, F., & Rhode, W. 2006, APh, 25, 118
Biehl, D., Boncioli, D., Fedynitch, A., & Winter, W. 2018, A&A, 611, A101
Bissaldi, E., Omodei, N., Kerr, M. & Fermi-LAT Team 2022, GCN, 32637, 1
Burns, E., Svinkin, D., Fenimore, E., et al. 2023, ApJL, 946, L31
Bustamante, M., Baerwald, P., Murase, K., & Winter, W. 2015, NatCo, 6, 6783
de Ugarte Postigo, A., Izzo, L., Pugliese, G., et al. 2022, GCN, 32648, 1
Dichiara, S., Gropp, J. D., Kennea, J. A., et al. 2022, GCN, 32632, 1
Feldman, G. J., & Cousins, R. D. 1998, PhRvD, 57, 3873
Gando, A., Gando, Y., Hachiya, T., et al. 2016, PhRvL, 117, 082503
Gando, A., Gando, Y., Hanakago, H., et al. 2013, PhRvD, 88, 033001
Gando, Y., Gando, A., Hachiya, T., et al. 2020, JPhCS, 1468, 012142
Gando, Y., Gando, A., Hachiya, T., et al. 2021, JInst, 16, P08023
Griswold, S., BenZvi, S., Uberoi, N., & Cross, R. 2020, IceCubeOpenSource/ASTERIA: v1.0.0, Zenodo, doi:10.5281/zenodo.3926835
Halzen, F., & Jaczko, G. 1996, PhRvD, 54, 2779
Huang, Y., Hu, S., Chen, S., et al. 2022, GCN, 32677, 1
Hümmer, S., Baerwald, P., & Winter, W. 2012, PhRvL, 108, 231101
Kistler, M. D., Haxton, W. C., & Yüksel, H. 2013, ApJ, 778, 81
Kruiswijk, K., Brinson, B., Procter-Murphy, R., Thwaites, J., & Valtonen-Mattila, N. 2023, arXiv:2307.16354
Lesage, S., Veres, P., Roberts, O. J., et al. 2022, GCN, 32642, 1
LHAASO Collaboration, Cao, Z., Aharonian, F., et al. 2023, Sci, 380, 1390
Lipari, P., & Vernetto, S. 2020, APh, 120, 102441
Liu, R.-Y., Zhang, H.-M., & Wang, X.-Y. 2023, ApJL, 943, L2
Liu, T., Gu, W.-M., & Zhang, B. 2017, NewAR, 79, 1
Murase, K. 2007, PhRvD, 76, 123001
Murase, K., Kashiyama, K., & Mészáros, P. 2013, PhRvL, 111, 131102
Murase, K., Mukhopadhyay, M., Kheirandish, A., Kimura, S. S., & Fang, K. 2022, ApJL, 941, L10
Murase, K., & Nagataki, S. 2006, PhRvD, 73, 063002
Mészáros, P., & Rees, M. J. 1997, ApJL, 482, L29
Pitik, T., Tamborra, I., Angus, C. R., & Auchettl, K. 2022, ApJ, 929, 163
Qi, Y.-Q., Liu, T., Huang, B.-Q., Wei, Y.-F., & Bu, D.-F. 2022, ApJ, 925, 43
Rees, M. J., & Meszaros, P. 1994, ApJL, 430, L93
Rudolph, A., Petropoulou, M., Winter, W., & Bosnjak, Z. 2023, ApJL, 944, L34
Strumia, A., & Vissani, F. 2003, PhLB, 564, 42
Svinkin, D., Frederiks, D., Ridnaia, A., et al. 2022, GCN, 32641, 1
Thomas, J. K., Moharana, R., & Razzaque, S. 2017, PhRvD, 96, 103004
Waxman, E., & Bahcall, J. 1997, PhRvL, 78, 2292
Waxman, E., & Bahcall, J. N. 2000, ApJ, 541, 707
Xu, D., de Ugarte Postigo, A., Leloudas, G., et al. 2013, ApJ, 776, 98
Zhang, B. T., Murase, K., Ioka, K., et al. 2023, ApJL, 947, L14